Remotely Sensed Vegetation Green-Up Onset Date on the Tibetan Plateau: Simulations and Future Predictions

Ruyin Cao, Xiaofang Ling, Licong Liu, Weiyi Wang, Luchun Li, and Miaogen Shen

***Abstract*—Vegetation green-up onset date (VGD) is a key indicator of ecosystem structure and processes. As the largest and highest alpine ecoregion, the Tibetan plateau (TP) has experienced markable climate warming during the past decades and showed substantial changes in VGD. However, the existing process-based phenology models still cannot simulate interannual variations in satellite-derived VGD. In this study, we developed a data-driven VGD model for the TP based on the Long short-term memory neural network (called VGD-LSTM). VGD-LSTM considers the complicated nonlinear relationship between VGD and multiple climatic and environmental drivers, including the time series of temperature (daytime, daily minimum, and daily mean) and precipitation, as well as nonsequential variables (elevation and geolocation). Compared with the benchmark process-based VGD model for the TP (i.e., the hierarchical model), VGD-LSTM greatly improved the simulation of interannual VGD variations. We calculated the correlation coefficients (R) between satellite-derived VGDs and VGD simulations during 2000–2018; the percentages of pixels with R values above 0.5 increased from 15% for the hierarchical model to 41% for VGD-LSTM. The advanced trend in the satellite-derived VGD on the entire TP during 2000–2018 (−0.37 day/year) was captured well by VGD-LSTM (−0.33 day/year) but was underestimated by the hierarchical model (−0.08 day/year). According to VGD-LSTM simulations, VGDs on the TP are projected to advance by 8–10 days by 2100 relative to 2015–2020 under high shared socioeconomic pathway scenarios. This study suggests the potential of artificial intelligence in phenology modeling for which the physiological processes are difficult to be fully represented.**

***Index Terms*—Alpine ecosystem, land surface phenology, phenological model, Qinghai–Tibet plateau, start of vegetation growing season.**

Manuscript received 13 March 2023; revised 13 June 2023; accepted 19 August 2023. Date of publication 31 August 2023; date of current version 13 September 2023. This work was supported in part by the Second Scientific Expedition to the Qinghai–Tibet Plateau under Grant 2019QZKK0307 and in part by the National Natural Science Foundation of China under Grant 42271379. *(Corresponding author: Ruyin Cao.)*

Ruyin Cao, Xiaofang Ling, Weiyi Wang, and Luchun Li are with the School of Resources and Environment, University of Electronic Science and Technology of China, Chengdu 611731, China (e-mail: cao.ruyin@uestc.edu.cn; lingxiaofang@std.uestc.edu.cn; 202221070117@std.uestc.edu.cn; 202121070118@std.uestc.edu.cn).

Licong Liu and Miaogen Shen are with the State Key Laboratory of Earth Surface Processes and Resource Ecology, Faculty of Geographical Science, Beijing Normal University, Beijing 100875, China (e-mail: liulicong@mail.bnu.edu.cn; shenmiaogen@bnu.edu.cn).

Digital Object Identifier 10.1109/JSTARS.2023.3310617

I. Introduction

VEGETATION phenology is the study of the periodically recurring change patterns of vegetation annual growth and development [1]. As an important phenological stage, vegetation green-up onset date (VGD) estimated from satellite observations characterizes the start time of increasing vegetation greenness and is recognized to be a key parameter that affects various ecosystem processes and functions, such as ecosystem carbon and water cycles [2], [3], plant community structure [4], [5], and the ecosystem feedback to climate systems [6], [7]. In the context of climate warming, VGD also appears to be a direct and sensitive vegetation indicator that exhibits an initial response [8]. The Tibetan Plateau (referred to as TP hereafter) is located in southwestern China (26°–39.8°N, 73.3°–104°E) and is the largest and highest alpine ecoregion in the world, covering over 2.5 million km^2, with an average elevation above 4000 m. Since the 1980s, the TP has experienced more rapid climate warming than the global average, with rates of increase of 0.27, 0.19, and 0.36 °C per decade in terms of the annual mean temperature, maximum temperature, and minimum temperature, respectively [9]. Because spring vegetation phenology in alpine ecosystems is expected to be highly sensitive to temperature changes [10], many studies have investigated the temporal shifts in VGD of the TP and their driving factors using both field phenological datasets and satellite observations (see reviews by Shen et al. [11]).

Generally, VGD on the TP is recognized to be mainly controlled by the heat accumulation in a period before VGD (i.e., preseason temperature; [12], [13]). Although the temporal shift in VGD averaged over the entire TP has exhibited an advancing trend during the past four decades, VGD was found to be postponed in some areas of the southwestern TP since 2000, which was attributed to limited water availability in these local semiarid areas [14]. Ganjurjav et al. [15] performed a manipulative experiment and found interactive effects of preseason temperature and precipitation on spring phenology on the TP: increasing preseason precipitation could offset the warming-induced delaying trend of spring phenology in drier areas. Winter temperature regulates VGD in some ecosystems (e.g., temperate forests) because a certain amount of low-temperature accumulation (chilling) is required to break endodormancy before starting ecodormancy [16]. Yu et al. [17] reported that insufficient fulfilment of the chilling requirements may explain the delayed VGD of the TP

during 1997–2006. However, some later studies argued against this assumption, as winter temperature is still rather low despite warming [18], [19]. Recently, several studies highlighted the asymmetric impacts of daytime and nighttime warming on VGD [20], [21], [22], [23], [24]. Unlike northern middle and high latitudes, where VGD is more sensitive to daytime temperature, VGD on the TP is more closely related to daily minimum temperature, which is hypothesized as a low-temperature constraint on plant development on this cold plateau [25], [26]. These findings suggest that asymmetric warming in the diurnal course is crucial to explore in our investigations of the temperature sensitivity of VGD.

Various climate drivers serve the development of phenology simulation models. There have been some attempts to simulate VGD of the TP, and the existing models are either process based or statistically regressed. The spring warming model is the simplest process-based phenology model, which considers only the influence of the accumulated preseason temperature and assumes that VGD occurs when the heat accumulation (S_f) reaches a critical value (F^*). It is generally formulated as follows:

$$S_f = \sum_{i=t_s}^{\mathrm{VGD}} \max\left(0, T_i - T_{\mathrm{base}}\right) \geq F^* \tag{1}$$

where T_i is the daily mean temperature at the ith day, T_{base} is the base temperature above which heat accumulation occurs, and t_s is the starting date for heat accumulation. The spring warming model was found to perform poorly for simulating VGD in grasslands due to the exclusion of other driving factors, such as preseason precipitation that has a strong influence on VGD in the southwestern TP [27], [28]. The temperature–precipitation coupling model of Chen et al. [27] assumes that both the heat requirement and the accumulated preseason precipitation should reach critical values to trigger VGD on the TP. They further evaluated both the air temperature–precipitation parallel model and the sequential model in which the start dates of the state of forcing in temperature and precipitation are assumed to occur parallelly or sequentially. Simulations for 18 herbaceous species at 19 phenological stations on the TP showed that the temperature–precipitation sequential model performed better than the parallel model at more phenological stations, highlighting the complex interactions between the heat and preseason precipitation accumulations [27]. Besides seasonal climate factors, the asymmetric influence of daytime and nighttime temperature was further considered in VGD simulations in a growing season index model [28], [29] and a hierarchical model [25]. The hierarchical model assumes spatially different climate drivers for VGD in different areas of the TP and, thus, includes five submodels (for details of the submodels, see Section II-C). It achieved a smaller mean absolute error (MAE) for VGD simulations across the entire TP than previous models.

The performances of current phenology models are still far from satisfactory [30], [31]. Because satellite observations provide phenology data with full coverage of space, it is possible to parameterize phenology models for each pixel [32], [33]. However, these phenology models still lack the ability to simulate interannual changes in VGD, which greatly limits our ability to predict future changes in VGD. In fact, it is easier to simulate spatial patterns of VGD owing to large spatial variations (e.g., $>$1 month for the TP), but it is much more difficult to capture temporal change trends in VGD due to small temporal variations in VGD [30]. A literature review revealed that few studies investigated the synchronization of the time-series data between the simulated and observed VGD. Liu et al. [34] evaluated the temporal trends in VGD simulation during 1982–2012 in the northern hemisphere obtained with multiple process-based phenology models and found that simulated VGD showed much smaller temporal trends than observed VGD. The poor performance of current process-based models could originate from the complex interactive influence of multiple factors on VGD that cannot be fully considered. For example, VGD is regulated by not only the sum but also the specific processes of thermal forcing [35], [36]. A more rapid increase rate in preseason temperature was shown to induce earlier VGD in a year even if the accumulated sum of preseason temperature in that year was smaller [35]. Besides thermal forcing, the time distribution and duration of precipitation may also affect VGD on the TP [18]. However, the subtle differences in the characteristics of these climate factors are difficult to incorporate into the process-based phenology models.

Machine learning techniques, particularly deep learning (DL) models, are increasingly being employed to estimate various environmental parameters [37]. The data-driven DL models potentially better approximate the complicated nonlinear relationship between the environmental parameters and climate factors, owing to multilayer learning through deep artificial neural networks [38]. Therefore, DL may be a promising tool to model the complex interactions of preseason temperature and precipitation on VGD. Zhou et al. [39] simulated global vegetation phenology during 2001–2015 by performing a DL-based experiment. Their one-dimensional (1-D) convolutional neural network regression model captures spatial patterns of VGD well, whereas the simulation of the interannual changes in VGD, even for simulation assessment at the hemispheric scale averaging over all pixels, seems to be less satisfactory (quantitative indices were not given in their Fig. S11). Toward VGD prediction on the TP, it is worth exploring a model with a more effective ability to simulate VGD, particularly the interannual changes in TPs VGD.

In this study, we, therefore, developed a data-driven phenology model based on the long short-term memory to simulate VGD on the TP (referred to as VGD-LSTM). Multiple climate drivers are incorporated into the VGD-LSTM model, including the time series of temperature (daytime, daily minimum, and daily mean) and precipitation from the previous winter season to the current spring season. The strong data mining ability of long short-term memory (LSTM) benefits the learning of multilevel features from these time-series data. We tested the performance of VGD-LSTM in simulating satellite-derived VGD on the TP, particularly with regard to modeling interannual variations in VGD. We also estimated future VGD changes on the TP until the end of this century by driving the VGD-LSTM model using climate projection from the Coupled Model Intercomparison Project Phase 6 (CMIP6) under four different shared socioeconomic pathway (SSP) scenarios [40].

TABLE I
DETAILS OF THE 13 CMIP6 MODELS USED IN THIS STUDY

Model name	Country / Region	Horizontal resolution	Reference
BCC-CSM2-MR	China	320×160	[45]
CanESM5	Canada	128×64	[46]
EC-Earth3	Europe	512×256	[47]
EC-Earth3-Veg	Europe	512×256	[48]
FGOALS-g3	China	180×90	[49]
GFDL-ESM4	USA	288×180	[50]
INM-CM4-8	Russia	180×120	[51]
INM-CM5-0	Russia	180×120	[52]
IPSL-CM6A-LR	France	144×143	[53]
MIROC6	Japan	256×128	[54]
MPI-ESM1-2-HR	German	384×192	[55]
MRI-ESM2-0	Japan	320×160	[56]
NorESM2-MM	Norway	288×192	[57]

II. MATERIALS AND METHODS

A. Climate Datasets on the TP

We collected the China meteorological forcing dataset (CMFD) to drive VGD simulations on the TP. The CMFD dataset was generated by the data assimilation and modeling center for multispheres, Institute of Tibetan Plateau Research, Chinese Academy of Sciences, and has been widely used in previous studies [41]. It provides air temperature and precipitation data for 1979–2018 with a temporal resolution of 3 h at a cell size of 0.1° × 0.1° (http://data.tpdc.ac.cn/en/data/8028b944-daaa-4511-8769-965612652c49/). Air temperatures were produced by merging station meteorological observations made by the China Meteorological Administration and the corresponding Princeton forcing data [42]. Precipitation data were produced from China Meteorological Administration station observations, tropical rainfall measuring mission satellite precipitation analysis data [43], and Asian precipitation−highly resolved observational data integration towards evaluation of water resources precipitation data [44]. In this study, we used only 2000–2018 climate data from CMFD because the MODIS observations date back to 2000.

To predict VGD changes under future climates on the TP, we collected the daily outputs of 13 climate models participating in the CMIP6. All 13 models (see Table I) provide four climate variables, including daily mean temperature ("tas"), daily maximum temperature ("tasmax"), daily minimum temperature ("tasmin"), and daily precipitation ("pr"), under four SSP scenarios (SSP1-2.6, SSP2-4.5, SSP3-7.0, and SSP5-8.5). There are still some missing data in some of the climate models. We processed these missing data as follows.

1) Some "tas" data are missing in the historical data (2000–2014) for BCC-CSM2-MR and CanESM5, and they were filled as "(tasmax+tasmin)/2."
2) Some "tasmin" data are missing in some years during 2021–2030 for NorESM2-MM under the SSP370 scenario, and they were filled as "2×tas - tasmax."
3) "tasmax" data are missing in 2034 and 2093 in FGOALS-g3, and they were filled as "2×tas - tasmin."

All these climate data were resampled to the same spatial resolution of 0.1° × 0.1° by the bilinear interpolation.

B. Satellite-Derived VGDs on the TP

To estimate VGD on the TP, we collected the 2000–2018 MODIS vegetation index (VI) product (MOD13A1, version 6) from the U.S. Geological Survey, which provides both the normalized difference vegetation index (NDVI) and the enhanced vegetation index (EVI) data with 250-m and 16-day spatiotemporal resolution. Although the maximum value composition technique has been applied to MOD13Q1, there is still residual noise in the original VI time-series data that needs to be processed [58], [59]. Specifically, we first filled the VI values contaminated by clouds and cloud shadows by the linear interpolation of the VI time series. We then followed Zhang et al. [60] to employ the background VI value of each pixel to replace the VI values contaminated by snow and ice in winter. The background VI value was determined as the average of historical high-quality VI values during the period from the previous December to the current March. Finally, we smoothed the VI time-series data using the Savitzky–Golay filter [61], [62].

We estimated VGD for only those vegetation pixels with seasonality of greenness on the TP. As suggested by previous studies, two criteria were adopted to screen these pixels: First, having multiple-year average VI values during July–September higher than a threshold (NDVI $>$ 0.1; [14]); and second, the July–September average NDVI value is larger than 1.1 times the average NDVI during December–February. These selected pixels with their vegetation types are shown in the upper panel of Fig. 1.

VGD was detected from NDVI and EVI time-series data using the threshold-based and inflection-point-based methods [63]. We used the double logistic functions to fit the VI time-series data of each pixel

$$\mathrm{VI}\ (t,m) = m_1\ + m_2\left(\frac{1}{1+e^{m_3-m_4 t}} + \frac{1}{1+e^{m_5-m_6 t}}\right) \tag{2}$$

where m_1–m_6 are the fitting parameters. VGD was determined as the first date when VI increases by 20% of its annual amplitude (i.e., relative threshold) or the date of the first local maximum in the rate of change of the curvature of the fitted logistic function (i.e., inflection point; [64]). VGD estimates from the two methods and two VIs were averaged to reduce uncertainty in estimates [11]. To be compatible with the spatial resolution of CMFD, we followed Shen et al. [11] to resample the VGD data to 0.1° × 0.1° by averaging all available VGD estimates within each 0.1° × 0.1° grid if their percentage within the grid exceeds 10%. The spatial distribution of the mean VGD during 2000–2018 exhibits a clear longitudinal pattern with delayed VGD from the eastern to western TP (Fig. 1, lower panel), which is generally consistent with previous observations [11], [65].

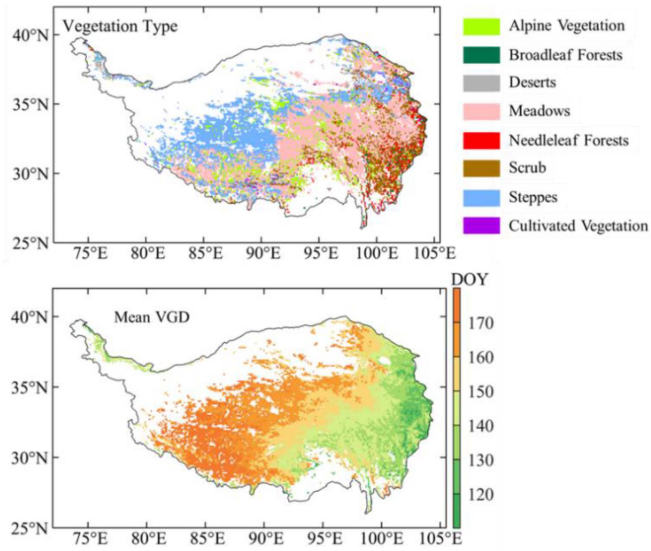

Fig. 1. Spatial distribution of vegetation types for the pixels with VGD estimates (upper) and the mean VGD estimates (0.1° × 0.1°) during 2000–2018 (lower).

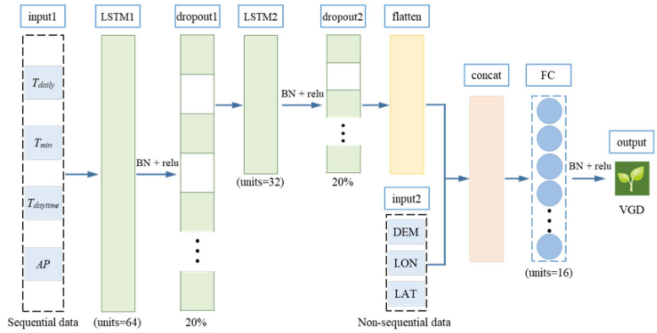

Fig. 2. Neural network structure of VGD-LSTM, which includes two input layers, two LSTM layers, two dropout layers, one flatten layer, one concatenate (concat) layer, one FC layer, and one output layer. BN: Batch normalization; relu: Rectified linear unit.

C. Previous Hierarchical Model for the TP

We employed the hierarchical model as the benchmark process-based model for comparisons, which was reported to perform better than other process-based models for VGD simulations on the TP [25]. The hierarchical model consists of five submodels, each with different combinations of dominant climate drivers. The candidate climate drivers include the preseason accumulated precipitation ($\boldsymbol{AP}$) and four temperature variables, daily mean temperature ($\boldsymbol{T_{daily}}$), daytime temperature ($\boldsymbol{T_{daytime}}$), and daily minimum temperature ($\boldsymbol{T_{\min}}$) during the preseason period, and the winter daily mean temperature ($\boldsymbol{T_{winter}}$). The dominant climate drivers for VGD simulations in each pixel are identified by the partial least square regression according to the variable importance in a partial least square regression projection. Using the satellite-derived VGD as the reference values, the hierarchical model was found to better simulate VGD on the TP than other phenology models, including the traditional one-phase spring warming model, the two-phase chilling-forcing model, and the temperature–precipitation parallel or sequential models. For the structure of the hierarchical model, refer to [25, Table I].

D. Proposed VGD-LSTM Model for the TP

As a variant of a recurrent neural network, the LSTM neural network adds a cell state parameterized structure and internal memory to store previous information, and it has proven to be more powerful in modeling and forecasting time series [66]. We proposed a two-layer LSTM neural network to simulate VGD on the TP (VGD-LSTM). Fig. 2 shows the network structure of VGD-LSTM, which is driven by the input data, including the time series of four climate variables (i.e., daytime, daily minimum, and daily mean temperature and precipitation) and the nonsequential variables (elevation, latitude, and longitude). These nonsequential variables were considered because they may affect the relationship between VGD and climate variables. For example, the thermal forcing threshold to trigger VGD may be affected by elevations and geographic locations [11].

For the network, we used the built-in algorithm hyperband [67] in Keras Tunner [68] to determine the best hyperparameters. The two unidirectional LSTM layers have 64 and 32 hidden units, respectively. We added the corresponding batch normalization and rectified linear unit to the network to avoid gradient vanishing and accelerate the convergence. A flattened layer was included to convert the extracted features to 1-D feature vectors and to further concatenate them with the nonsequential variables (see Fig. 2). In addition, we added the dropout layer after each LSTM layer to improve the generalization of the network. The ratio value in the dropout layer was set to be 0.2, meaning that 20% of the parameters of each layer will be removed from training in each iteration. A fully connected (FC) layer followed by an activation function (i.e., rectified linear unit) was added to integrate features to give the prediction of VGD. The VGD-LSTM model uses a total of 100 epochs and a batch size of 256.

Since VGD on the TP normally occurs before the end of July, the input time series of four climate variables has a length of 300 days from October of the previous year to July of the current year. To reduce the number of model parameters, the original daily climate variables were composited to 3 days, forming 100-D data for each climate variable. Both the input climate variables and the input nonsequential variables were normalized to [0, 1] using their respective minimum and maximum values. The network parameters were optimized with the Adam (adaptive moment estimation) optimization algorithm [69] by minimizing the root-mean-square error between model-estimated and satellite-derived VGDs. We used an initial network learning rate of 0.001, and then changed it dynamically according to the network iterations: when the loss of the validation set after two iterations does not drop, the learning rate is reduced by 10%. The settings of the training set, validation set, and testing set in our experiments are described in Section III.

III. Experiments and Assessments

We compared the proposed VGD-LSTM model with the previous hierarchical model in terms of the performance of VGD simulations on the TP using the climate dataset CMFD (2000–2018). To make the evaluations more robust, we adopted the leave-one-out cross-validation method. For the hierarchical model, every time we chose VGD data in 1 year from the total of 19 years (2000–2018) as the testing data, we used the VGD data in the remaining 18 years to calibrate the phenology model (i.e., parametrization) at each pixel. The optimal parameters were estimated by a genetic algorithm (sko. GA) in the scikit-opt-0.6.3 package of Python-3.7.6. For the VGD-LSTM model, every time we chose VGD data in two continuous years as the testing and validation datasets, respectively, and the VGD data in the remaining 17 years were used as the training dataset. For example, when using VGD data in 2000 as the testing dataset, we trained the VGD-LSTM model with the VGD data during 2002–2018 by setting the VGD data in 2001 as the validation dataset. An exception is the case of the testing dataset in 2018, where VGD data in 2017 were chosen as the validation dataset. We performed quantitative assessments by comparing VGD simulations with testing datasets. Two statistical indices were used, including the MAE and correlation coefficient (R).

We further employed the VGD-LSTM model and the hierarchical model to simulate the projections of VGD under future climate scenarios provided by the 13 CMIP6 climate models with four SSP scenarios. The hierarchical models were calibrated for different CMIP6 climate models using the corresponding historical simulations (2000–2014). The VGD-LSTM model for each CMIP6 climate model was trained with the VGD data in the historical period (2000–2013) by setting the VGD data in 2014 as the validation dataset. We investigated the projections of VGD during 2015–2100 on the TP simulated by VGD-LSTM and the hierarchical model.

IV. Results

Fig. 3 shows the spatial distribution of the MAE values for VGD simulations by the VGD-LSTM and hierarchical models. Notably, the experiments were conducted using the leave-one-out method in which we simulated VGD year-by-year. For each pixel in Fig. 3, the MAE value was averaged over 19 years (2000–2018). In general, most of the areas on the TP have MAE values between 4 and 8 days except some local areas in the southwestern TP with values larger than 10 days. This spatial pattern is unrelated to vegetation types (cf. Fig. 3 and upper panel in Fig. 1). The VGD-LSTM performed slightly better than the hierarchical model in terms of the absolute difference between VGD simulations and satellite-derived VGD observations (mean MAE: 7.03 versus 7.18 days).

We further investigated the performance of the VGD-LSTM and the hierarchical models in simulating the interannual variations in VGD for each pixel. We calculated Pearson's correlation coefficients (R) between VGD simulations and satellite-derived VGD observations for 2000–2018. Results show that VGD-LSTM performed obviously better than the hierarchical model [R averaged over all pixels: 0.431 versus 0.105; Fig. 4(a) and (b)]. For the VGD-LSTM model, the percentages of pixels with R values between 0.2 and 0.5 and >0.5 are 46% and 41%, respectively, whereas the percentages are only 27% and 15% for the hierarchical model. VGD-LSTM successfully simulated the interannual VGD variations (i.e., a significant positive correlation, $P < 0.05$) for about 50% of the pixels, whereas only 24% of the pixels showed a significant positive correlation for the hierarchical model [see Fig. 4(c) and (d)]. Previous studies also reported that the process-based phenology models lack the ability to capture the interannual variations in VGD on the TP (see [25, Fig. 5]). This great improvement provided by the VGD-LSTM allows us to predict the variations of VGD on the TP under future changing climates.

We averaged the satellite-derived VGD data or VGD simulations over all pixels on the TP for each year and investigated

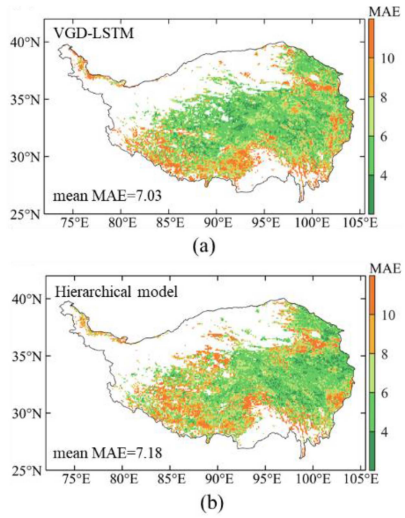

Fig. 3. Spatial distribution of the MAE values for VGD simulations. The MAE value for each pixel is averaged over 19 years (2000–2018) because we adopted the leave-one-out cross-validation method. The mean MAE shown in each panel was averaged across all pixels.

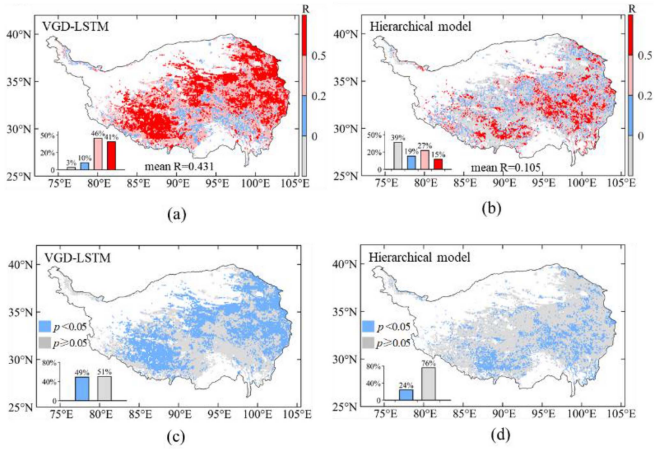

Fig. 4. (a) and (b) Spatial distribution of the correlation coefficient (R) values for VGD simulations. The R value of each pixel is calculated between VGD simulations and satellite-derived VGD observations during 2000–2018. The mean R was averaged across all pixels. (c) and (d) Spatial distribution of pixels with a significant R ($P < 0.05$).

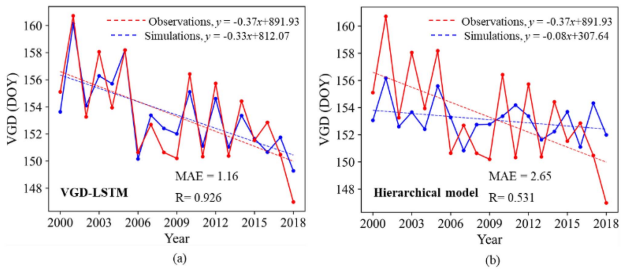

Fig. 5. Time series of satellite-derived VGD observations (red line) and VGD simulations (blue line) averaged over the TP during 2000–2018. The MAE and correlation coefficient (R) between VGD observations and simulations are shown in each panel.

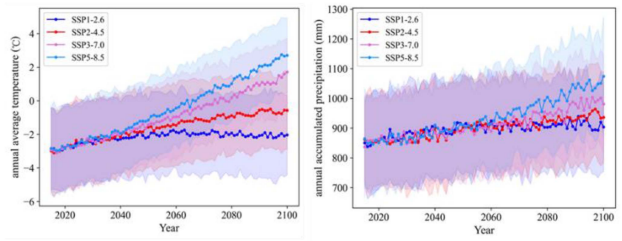

Fig. 6. Projected annual mean temperature and accumulated precipitation on the TP under SSP1-2.6, SSP2-4.5, SSP3-7.0, and SSP5-8.5, based on the CMIP6 multimodel ensemble. The ranges indicated by light color represent the standard deviation of predictions from the 13 CMIP6 climate models (see Table I).

the synchronization between time series of the two datasets (see Fig. 5). Results show that VGD on the TP exhibited an advanced trend during 2000–2018 at a rate of 3.7 days per decade ($P < 0.05$). This temporally advanced trend was well captured by the VGD-LSTM (3.3 days per decade, $P < 0.05$) but was greatly underestimated by the hierarchical model (0.8 days per decade, $P > 0.05$). The correlation coefficient between VGD observations and VGD simulations is >0.92 for VGD-LSTM, further highlighting the robustness of the new data-driven phenology model.

Fig. 6 shows the projected annual mean temperature and accumulated precipitation from the CMIP6 multimodel ensemble under SSP1-2.6, SSP2-4.5, SSP3-7.0, and SSP5-8.5. The annual mean temperature on the TP is expected to increase with an amplitude of approximately 6 °C (from −3 to 3 °C) under SSP5-8.5 (high greenhouse gas emission) by 2100. Under SSP1-2.6 (low greenhouse gas emission), however, the increase in annual mean temperature halts around 2040. Regarding annual accumulated precipitation, more substantial increases were observed under SSP5-8.5 and SSP3-7.0 than in the other two scenarios.

We employed the proposed VGD-LSTM model to predict the TPs VGD changes from 2015 to 2100 under future climates (see Fig. 7). Relative to 2015–2020, the averaged VGD is projected to advance by 8–10 days by 2100 under the relatively high greenhouse gas emission scenarios (SSP3-7.0 and SSP5-8.5). However, under the low-emission scenarios (SSP1-2.6), VGD is projected to slightly advance before 2040 and then this trend will be halted.

We further examined the spatial distributions of projected VGD changes between the mean VGD in 2015–2020 and that in 2095–2100 (see Fig. 8). Under the SSP5-8.5 scenario, VGD predicted by VGD-LSTM exhibits evident spatial heterogeneity.

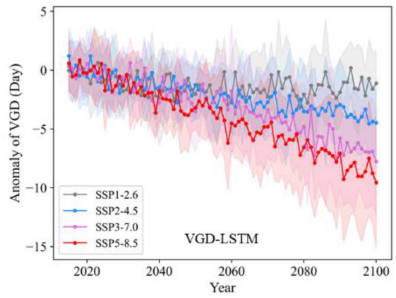

Fig. 7. Relative to 2015–2020, projected future VGD until 2100 averaged over all pixels under SSP1-2.6, SSP2-4.5, SSP3-7.0, and SSP5-8.5, based on the CMIP6 multimodel ensemble. The ranges indicated by light color represent the standard deviation of VGD predictions using 13 CMIP6 climate models.

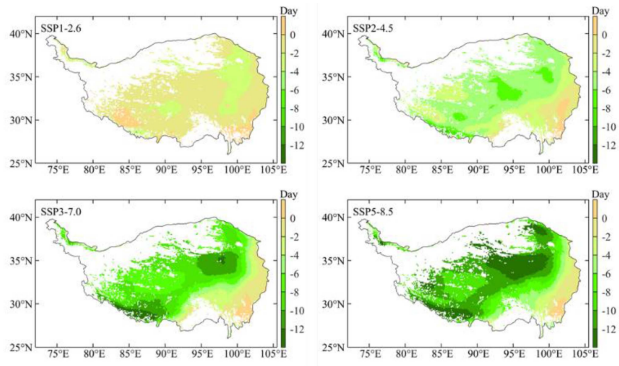

Fig. 8. Spatial distributions of projected VGD in 2095–2100 relative to 2015–2020 under the SSP1-2.6, SSP2-4.5, SSP3-7.0, and SSP5-8.5, based on the CMIP6 multimodel ensemble.

It can be observed that VGD in 2095–2100 relative to 2015–2020 advanced by more than 10 days in most areas in the western and southwestern TP (negative values in Fig. 8), but this more obvious advanced trend was offset by a delayed trend for some areas in the eastern TP (positive values in Fig. 8) when all pixels on the TP were averaged. The interesting delay in VGD in the VGD-LSTM predictions in some eastern areas was due to the combined effect of multiple climate variables, which will be further explained in Section V-B (see Fig. 9).

V. Discussion

A. Performances of VGD Simulations by VGD-LSTM

The correlations between VGD on the TP and various environmental factors have been documented in many studies, but current process-based phenology models still perform poorly in VGD simulations, particularly in the simulation of interannual VGD variations [11]. One reason may be due to the lack of mechanistic understanding of different drivers, such as the roles of winter chilling and the interactive effects between temperature and precipitation on VGD. In addition to accumulated temperature and precipitation, the temporal distribution of precipitation and the specific processes of thermal forcing at daily time scales were also found to affect VGD [26], [35], [36]. Apparently, the complex effects of these driving factors on VGD are difficult to properly express in the process-based phenology models because these models can normally include at most three or four climate variables (e.g., two-phase phenology models). In

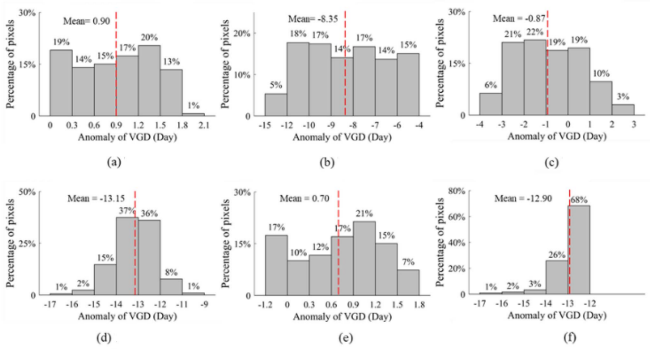

Fig. 9. Histogram distribution of projected relative changes in VGD in the ablation experiment (2095–2100 relative to 2015–2020). We show the (a) original data and the (b) exchange of the time series of temperature, (c) precipitation, (d) both temperature and precipitation, (e) nonsequential variables, and (f) all variables. The red dashed line in each panel represents the mean value of the projected relative changes in VGD.

contrast, as a DL-based phenology model, VGD-LSTM has the ability to characterize the influence of the time-series process of multiple climate variables on VGD (see Fig. 2). Our experiments showed that the simulations of interannual variations in VGD have been substantially improved by the VGD-LSTM model. About 50% of pixels have a significant positive correlation between satellite-derived and simulated VGD when using VGD-LSTM, but only 24% do for the previous hierarchical model (see Fig. 4). The advanced trend in the satellite-derived VGD on the entire TP during 2000–2018 (0.37 day/year, $P < 0.05$) was captured well by the VGD-LSTM model (0.33 day/year, $P < 0.05$; Fig. 5).

The VGD-LSTM model has many more parameters than the process-based hierarchical model. Thus, there may be concern whether the performance of VGD-LSTM was exaggerated due to model overfitting. Notably, some recent phenology studies adopted the spatial sampling strategy to calibrate and validate phenology models (e.g., [33] and [39]). They selected different pixels with spatial random sampling or uniform sampling to generate the training, validation, and testing sets; however, the selected pixels in the three sets may not be independent of each other owing to spatial autocorrelations, resulting in an overestimation of phenology model performance. To address this issue, we adopted the leave-one-out cross-validation strategy to test VGD-LSTM in which every time VGD data in one year were used as the testing set, VGD data in another year were used as the validation set, and VGD data in the remaining years were used as the training set. Although this strategy is very time-consuming, it ensures a robust assessment of the model's performance [70].

B. Projections of VGD Under CMIP6 Models

We applied VGD-LSTM to simulate the projections of VGD until the end of this century under four SSP scenarios based on the ensemble of 13 CMIP6 climate models. Relative to 2015–2020, VGD averaged over all pixels during 2095–2100 is predicted in advance by 8–10 days under SSP5-8.5 and by 1–2 days under SSP1-2.6 (see Fig. 7), which is generally consistent with the prediction of the hierarchical model in a recent study [11]. However, the spatial distributions of projected VGD changes are substantially different between the two phenology models (cf. Fig. 8 and [11, Fig. S3]). VGD predicted by VGD-LSTM does not exhibit advanced trends in some eastern areas by 2100 even under the high greenhouse gas emission scenario (SSP5-8.5). Here, we conducted an additional ablation experiment to examine which of the driving factors account for this observation. Specifically, we first selected the pixels with positive relative changes (values > 0 in Fig. 8, referred to as "Pixels > 0") and the pixels with relative changes smaller than -12 (values < -12 in Fig. 8, referred to as "Pixels < -12"). For each pixel in "Pixels > 0," we then replaced the driving factors (time series of climate variables or nonsequential variables) with the corresponding driving factors of a randomly selected pixel in "Pixels < -12." Based on the replaced driving factors, we used VGD-LSTM to simulate the projections of VGD until 2100 for all pixels in "Pixels > 0" again. Our results show that the original VGD relative changes with a mean value of 0.90 day decrease to a mean value of -8.35 days and -0.87 day when only the time-series data of temperature or precipitation were replaced, respectively [see Fig. 9(b) and (c)]. If the temperature and precipitation time-series data were replaced simultaneously, the mean value of VGD relative changes further decrease to -13.15 days [see Fig. 9(d)]. In contrast, the original VGD relative changes vary little when only nonsequential variables related to vegetation type (elevation, latitude, and longitude) were replaced [see Fig. 9(e)], suggesting that local climates, not vegetation types, are the main factors determining the spatial heterogeneity of the projections of VGD from VGD-LSTM. This additional experiment highlights the influence of the temporal profiles of intra-annual temperature and precipitation and the complex interactions between the two variables on VGD. However, we should acknowledge great uncertainties in the prediction of daily temperature and precipitation data by current climate models, being the main obstacle besides phenology models for reliable VGD simulations.

C. Limitations in the Simulations of VGD-LSTM

Several limitations remain in the simulations of VGD-LSTM. First, the physiological mechanisms controlling VGD are difficult to explain with the VGD-LSTM model because of the well-known black box problem for data-driven DL models. For example, VGD-LSTM still lacks the ability to reveal the specific processes and mechanisms underlying the complex interactions between the time series of temperature and precipitation. The coupling of process-based field physiological experiments and machine learning models might provide a solution to further reduce the uncertainties in VGD simulations and predictions in the future [71], [72]. Second, it is impossible to include all driving factors in phenology models. The VGD-LSTM model includes the main drivers (temperature and precipitation) as the direct inputs and considers some other climate and environmental variables indirectly. For example, VGD-LSTM includes the precipitation time-series data since October 1 of the previous year, suggesting the considerations of the influence of winter snowfall on VGD. However, the mechanism for this influence

is still unclear because of the large time interval (nearly two months) between spring snow melt date and VGD on the TP [11]. Photoperiod is also considered in VGD-LSTM to some extent when using the geographic locations (longitude and latitude) as inputs. However, the effects of livestock grazing [73] and nitrogen addition [74] on VGD are not considered because these data are difficult to collect and parameterize across the entire TP. Third, the projections of VGD until 2100 should be treated with caution due to uncertainties in the performance of phenology models and in the projected future climate scenarios in CMIP6. Although VGD-LSTM improved the simulations of interannual VGD variations, the performance for about half the pixels was still poor (see Fig. 4). Moreover, vegetation adaptation to future climate changes is not considered in the VGD predictions. Fourth, the performance of VGD-LSTM may be further improved by using longer VGD time-series data to train the model. Currently, VGD on the TP since 1982 can be estimated from the advanced very-high-resolution radiometer (AVHRR) NDVI time-series data. However, sensor degradation in AVHRR and the inconsistency among different generations of AVHRR sensors greatly hinder the application of this satellite dataset [75]. Therefore, more accurate MODIS data since 2000 were used in this study.

VI. Conclusion

We utilized the strong learning ability of the LSTM neural network and developed a DL-based phenology model to simulate VGD across the TP (VGD-LSTM). We tested the performance of VGD-LSTM with the leave-one-out cross-validation method for simulating VGD on the TP. By comparing the new model with the benchmark process-based model, VGD-LSTM performed slightly better than the hierarchical model developed for TP in terms of MAE error, but the simulations of interannual variations in VGD were substantially improved. Pearson's correlation coefficients (R) between satellite-derived VGDs and VGD simulations during 2000–2018 exhibit significant positive values ($P < 0.05$) in only 24% of the pixels for the hierarchical model but was improved to 49% of the pixels for VGD-LSTM. By averaging VGD over all vegetation pixels on the TP, VGD-LSTM achieved better synchronization between the time series of satellite-derived and simulated VGDs than the hierarchical model (R: 0.926 versus 0.531; Fig. 5), suggesting the effectiveness of the new data-driven phenology model. We further applied VGD-LSTM to estimate VGD changes on the TP in the 21st century by using climate projection from 13 CMIP6 models under four SSP scenarios. Results from an ensemble of 13 CMIP6 models project that, relative to 2015–2020, VGD averaged over all pixels will advance by 8–10 days by 2100 under high greenhouse gas emission scenarios (SSP3-7.0 and SSP5-8.5), whereas the advanced trend in VGD will be halted around 2040 under the low-emission scenario (SSP1-2.6). Because VGD is a key ecosystem parameter, we expect that more realistic simulation of VGD by VGD-LSTM can further improve our understanding of the influence of the Asian monsoon system on the TPs terrestrial ecosystem processes.

Data Availability Statement

The China meteorological forcing dataset is available from the National Tibetan Plateau Third Pole Environment Data Center (http://data.tpdc.ac.cn/en/data/8028b944-daaa-4511-8769-965612652c49/). Climate models' outputs are available via https://esgf-node.llnl.gov/search/cmip6/.MODIS, vegetation index (VI) product (MOD13A1, version 6) is provided by the U.S. Geological Survey.

References

[1] H. Lieth, *Phenology and Seasonality Modeling*, vol. 8. Berlin, Germany: Springer, 2013.

[2] S.-J. Jeong, D. Medvigy, E. Shevliakova, and S. Malyshev, "Uncertainties in terrestrial carbon budgets related to spring phenology," *J. Geophysical Res., Biogeosci.*, vol. 117, no. G1, 2012, Art. no. G01030, doi: 10.1029/2011JG001868.

[3] Y. Liu, C. Wu, X. Wang, R. S. Jassal, and A. Gonsamo, "Impacts of global change on peak vegetation growth and its timing in terrestrial ecosystems of the continental US," *Glob. Planet. Change*, vol. 207, 2021, Art. no. 103657, doi: 10.1016/j.gloplacha.2021.103657.

[4] L. H. Yang and V. H. W. Rudolf, "Phenology, ontogeny and the effects of climate change on the timing of species interactions," *Ecol. Lett.*, vol. 13, no. 1, pp. 1–10, 2010, doi: 10.1111/j.1461-0248.2009.01402.x.

[5] E. M. Wolkovich and M. J. Donahue, "How phenological tracking shapes species and communities in non-stationary environments," *Biol. Rev. Cambridge Philos. Soc.*, vol. 96, no. 6, pp. 2810–2827, 2021, doi: 10.1111/brv.12781.

[6] A. D. Richardson, T. F. Keenan, M. Migliavacca, Y. Ryu, O. Sonnentag, and M. Toomey, "Climate change, phenology, and phenological control of vegetation feedbacks to the climate system," *Agricultural Forest Meteorol.*, vol. 169, pp. 156–173, 2013, doi: 10.1016/j.agrformet.2012.09.012.

[7] X. Xiyan, W. J. Riley, C. D. Koven, J. Gensuo, and X. Zhang, "Earlier leaf-out warms air in the north," *Nature Climate Change*, vol. 10, no. 4, pp. 370–375, 2020, doi: 10.1038/s41558-020-0713-4.

[8] C. Körner and D. Basler, "Phenology under global warming," *Science*, vol. 327, no. 5972, pp. 1461–1462, 2010, doi: 10.1126/science.1186473.

[9] Q. You, J. Min, and S. Kang, "Rapid warming in the Tibetan plateau from observations and CMIP5 models in recent decades: Observation and simulations of warming," *Int. J. Climatol.*, vol. 36, no. 6, pp. 2660–2670, 2016, doi: 10.1002/joc.4520.

[10] J. Prevéy et al., "Greater temperature sensitivity of plant phenology at colder sites: Implications for convergence across northern latitudes," *Glob. Change Biol.*, vol. 23, no. 7, pp. 2660–2671, 2017, doi: 10.1111/gcb.13619.

[11] M. Shen et al., "Plant phenology changes and drivers on the Qinghai–Tibetan plateau," *Nature Rev. Earth Environ.*, vol. 3, no. 10, pp. 633–651, 2022, doi: 10.1038/s43017-022-00317-5.

[12] S. Piao et al., "Altitude and temperature dependence of change in the spring vegetation green-up date from 1982 to 2006 in the Qinghai-Xizang plateau," *Agricultural Forest Meteorol.*, vol. 151, no. 12, pp. 1599–1608, 2011, doi: 10.1016/j.agrformet.2011.06.016.

[13] X. Wang et al., "No consistent evidence for advancing or delaying trends in spring phenology on the Tibetan plateau," *J. Geophysical Res., Biogeosci.*, vol. 122, no. 12, pp. 3288–3305, 2017, doi: 10.1002/2017JG003949.

[14] M. Shen, G. Zhang, N. Cong, S. Wang, W. Kong, and S. Piao, "Increasing altitudinal gradient of spring vegetation phenology during the last decade on the Qinghai–Tibetan plateau," *Agricultural Forest Meteorol.*, vol. 189–190, pp. 71–80, 2014, doi: 10.1016/j.agrformet.2014.01.003.

[15] H. Ganjurjav et al., "Warming and precipitation addition interact to affect plant spring phenology in alpine meadows on the central Qinghai-Tibetan plateau," *Agricultural Forest Meteorol.*, vol. 287, 2020, Art. no. 107943, doi: 10.1016/j.agrformet.2020.107943.

[16] I. Chuine, X. Morin, H. Bugmann, C. Körner, and D. Basler, "Warming, photoperiods, and tree phenology," *Science*, vol. 32s9, no. 5989, pp. 277–278, 2010, doi: 10.1126/science.329.5989.277-e.

[17] H. Yu, E. Luedeling, and J. Xu, "Winter and spring warming result in delayed spring phenology on the Tibetan plateau," *Proc. Nat. Acad. Sci.*, vol. 107, pp. 22151–22156, 2010.

[18] M. Shen, S. Piao, N. Cong, G. Zhang, and I. A. Janssens, "Precipitation impacts on vegetation spring phenology on the Tibetan plateau," *Glob. Change Biol.*, vol. 21, no. 10, pp. 3647–3656, Oct. 2015, doi: 10.1111/gcb.12961.

[19] G. Zhang, Y. Zhang, J. Dong, and X. Xiao, "Green-up dates in the Tibetan plateau have continuously advanced from 1982 to 2011," *Proc. Nat. Acad. Sci.*, vol. 110, no. 11, pp. 4309–4314, Mar. 2013, doi: 10.1073/pnas.1210423110.

[20] Y. H. Fu et al., "Three times greater weight of daytime than of night-time temperature on leaf unfolding phenology in temperate trees," *New Phytologist*, vol. 212, no. 3, pp. 590–597, Nov. 2016, doi: 10.1111/nph.14073.

[21] L. Meng et al., "Divergent responses of spring phenology to daytime and nighttime warming," *Agricultural Forest Meteorol.*, vol. 281, 2020, Art. no. 107832, doi: 10.1016/j.agrformet.2019.107832.

[22] S. Piao et al., "Leaf onset in the northern hemisphere triggered by daytime temperature," *Nature Commun.*, vol. 6, no. 1, 2015, Art. no. 6911, doi: 10.1038/ncomms7911.

[23] S. Rossi and N. Isabel, "Bud break responds more strongly to daytime than night-time temperature under asymmetric experimental warming," *Glob. Change Biol.*, vol. 23, no. 1, pp. 446–454, 2017, doi: 10.1111/gcb.13360.

[24] G. Zhu et al., "Daytime and nighttime warming has no opposite effects on vegetation phenology and productivity in the northern hemisphere," *Sci. Total Environ.*, vol. 822, 2022, Art. no. 153386, doi: 10.1016/j.scitotenv.2022.153386.

[25] R. Cao, M. Shen, J. Zhou, and J. Chen, "Modeling vegetation green-up dates across the Tibetan plateau by including both seasonal and daily temperature and precipitation," *Agricultural Forest Meteorol.*, vol. 249, pp. 176–186, 2018, doi: 10.1016/j.agrformet.2017.11.032.

[26] M. Shen et al., "Strong impacts of daily minimum temperature on the green-up date and summer greenness of the Tibetan plateau," *Glob. Change Biol.*, vol. 22, no. 9, pp. 3057–3066, Sep. 2016, doi: 10.1111/gcb.13301.

[27] X. Chen, S. An, D. W. Inouye, and M. D. Schwartz, "Temperature and snowfall trigger alpine vegetation green-up on the world's roof," *Glob. Change Biol.*, vol. 21, no. 10, pp. 3635–3646, Oct. 2015, doi: 10.1111/gcb.12954.

[28] X. Chai et al., "Carbon flux phenology and net ecosystem productivity simulated by a bioclimatic index in an alpine steppe-meadow on the Tibetan plateau," *Ecol. Model.*, vol. 394, pp. 66–75, 2019, doi: 10.1016/j.ecolmodel.2018.12.024.

[29] Q. Sun et al., "A prognostic phenology model for alpine meadows on the Qinghai–Tibetan plateau," *Ecol. Indicators*, vol. 93, pp. 1089–1100, 2018, doi: 10.1016/j.ecolind.2018.05.061.

[30] S. Li et al., "Deficiencies of phenology models in simulating spatial and temporal variations in temperate spring leaf phenology," *J. Geophysical Res., Biogeosci.*, vol. 127, no. 3, 2022, Art. no. e2021JG006421, doi: 10.1029/2021JG006421.

[31] H. Zhao, Y. H. Fu, X. Wang, Y. Zhang, Y. Liu, and I. A. Janssens, "Diverging models introduce large uncertainty in future climate warming impact on spring phenology of temperate deciduous trees," *Sci. Total Environ.*, vol. 757, 2021, Art. no. 143903, doi: 10.1016/j.scitotenv.2020.143903.

[32] X. Yang, J. F. Mustard, J. Tang, and H. Xu, "Regional-scale phenology modeling based on meteorological records and remote sensing observations," *J. Geophysical Res., Biogeosci.*, vol. 117, no. G3, 2012, Art. no. G03029, doi: 10.1029/2012JG001977.

[33] L. Zheng, Y. Qi, Y. Wang, J. Peng, and Z. Qin, "Calibration and validation of phenological models for biome-BGCMuSo in the grasslands of Tibetan plateau using remote sensing data," *Agricultural Forest Meteorol.*, vol. 322, 2022, Art. no. 109001, doi: 10.1016/j.agrformet.2022.109001.

[34] Q. Liu, Y. H. Fu, Y. Liu, I. A. Janssens, and S. Piao, "Simulating the onset of spring vegetation growth across the northern hemisphere," *Glob. Change Biol.*, vol. 24, no. 3, pp. 1342–1356, 2018, doi: 10.1111/gcb.13954.

[35] M. A. Friedl et al., "A tale of two springs: Using recent climate anomalies to characterize the sensitivity of temperate forest phenology to climate change," *Environ. Res. Lett.*, vol. 9, no. 5, 2014, Art. no. 054006, doi: 10.1088/1748-9326/9/5/054006.

[36] C. Wang, R. Cao, J. Chen, Y. Rao, and Y. Tang, "Temperature sensitivity of spring vegetation phenology correlates to within-spring warming speed over the northern hemisphere," *Ecol. Indicators*, vol. 50, pp. 62–68, 2015, doi: 10.1016/j.ecolind.2014.11.004.

[37] Q. Yuan et al., "Deep learning in environmental remote sensing: Achievements and challenges," *Remote Sens. Environ.*, vol. 241, 2020, Art. no. 111716, doi: 10.1016/j.rse.2020.111716.

[38] Y. LeCun, Y. Bengio, and G. Hinton, "Deep learning," *Nature London*, vol. 521, no. 7553, pp. 436–444, 2015, doi: 10.1038/nature14539.

[39] X. Zhou, Q. Xin, Y. Dai, W. Li, and H. Qiao, "A deep-learning-based experiment for benchmarking the performance of global terrestrial vegetation phenology models," *Glob. Ecol. Biogeogr.*, vol. 30, no. 11, pp. 2178–2199, 2021, doi: 10.1111/geb.13374.

[40] V. Eyring et al., "Overview of the coupled model intercomparison project phase 6 (CMIP6) experimental design and organization," *Geosci. Model Develop.*, vol. 9, no. 5, pp. 1937–1958, 2016, doi: 10.5194/gmd-9-1937-2016.

[41] W. Tang et al., "China meteorological forcing dataset—Monthly," figshare, 2019, doi: 10.6084/m9.figshare.11397792.

[42] J. Sheffield, G. Goteti, and E. F. Wood, "Development of a 50-year high-resolution global dataset of meteorological forcings for land surface modeling," *J. Climate*, vol. 19, no. 13, pp. 3088–3111, 2006, doi: 10.1175/JCLI3790.1.

[43] G. J. Huffman et al., "The TRMM multisatellite precipitation analysis (TMPA): Quasi-global, multiyear, combined-sensor precipitation estimates at fine scales," *J. Hydrometeorol.*, vol. 8, no. 1, pp. 38–55, 2007, doi: 10.1175/JHM560.1.

[44] A. Yatagai, O. Arakawa, K. Kamiguchi, H. Kawamoto, M. I. Nodzu, and A. Hamada, "A 44-year daily gridded precipitation dataset for Asia based on a dense network of rain gauges," *Sci. Online Lett. Atmos.*, vol. 5, pp. 137–140, 2009, doi: 10.2151/sola.2009-035.

[45] X. Xin et al., "BCC BCC-CSM2MR model output prepared for CMIP6 CMIP," Earth Syst. Grid Federation, 2018, doi: 10.22033/esgf/cmip6.1725.

[46] N. C. Swart et al., "CCCma CanESM5 model output prepared for CMIP6 CMIP," Earth Syst. Grid Federation, 2019, doi: 10.22033/esgf/cmip6.1303.

[47] E. C.-E. Consortium, "EC-Earth-consortium EC-Earth3 model output prepared for CMIP6 CMIP," Earth Syst. Grid Federation, 2019a, doi: 10.22033/esgf/cmip6.181.

[48] E. C.-E. Consortium, "EC-Earth-consortium EC-Earth3-veg model output prepared for CMIP6 CMIP," Earth Syst. Grid Federation, 2019b, doi: 10.22033/esgf/cmip6.642.

[49] L. Li, "CAS FGOALS-g3 model output prepared for CMIP6 CMIP," Earth Syst. Grid Federation, 2019, doi: 10.22033/esgf/cmip6.1783.

[50] J. P. Krasting et al., "NOAA-GFDL GFDL-ESM4 model output prepared for CMIP6 CMIP," Earth Syst. Grid Federation, 2018, doi: 10.22033/esgf/cmip6.1407.

[51] E. Volodin et al., "INM INM-CM4-8 model output prepared for CMIP6 CMIP," Earth Syst. Grid Federation, 2019a, doi: 10.22033/esgf/cmip6.1422.

[52] E. Volodin et al., "INM INM-CM5-0 model output prepared for CMIP6 CMIP," Earth Syst. Grid Federation, 2019b, doi: 10.22033/esgf/cmip6.1423.

[53] O. Boucher et al., "IPSL IPSL-CM6A-LR model output prepared for CMIP6 CMIP," Earth Syst. Grid Federation, 2018, doi: 10.22033/esgf/cmip6.1534.

[54] H. Tatebe and M. Watanabe, "MIROC MIROC6 model output prepared for CMIP6 CMIP," Earth Syst. Grid Federation, 2018, doi: 10.22033/esgf/cmip6.881.

[55] J. Jungclaus et al., "MPI-M MPIESM1.2-HR model output prepared for CMIP6 CMIP," Earth Syst. Grid Federation, 2019, doi: 10.22033/esgf/cmip6.741.

[56] S. Yukimoto et al., "MRI MRI-ESM2.0 model output prepared for CMIP6 CMIP," Earth Syst. Grid Federation, 2019, doi: 10.22033/esgf/cmip6.621.

[57] M. Bentsen et al., "NCC NorESM2-MM model output prepared for CMIP6 CMIP," Earth Syst. Grid Federation, 2019, doi: 10.22033/esgf/cmip6.506.

[58] C. Wang, J. Chen, Y. Tang, T. A. Black, and K. Zhu, "A novel method for removing snow melting-induced fluctuation in GIMMS NDVI3g data for vegetation phenology monitoring: A case study in deciduous forests of North America," *IEEE J. Sel. Topics Appl. Earth Observ. Remote Sens.*, vol. 11, no. 3, pp. 800–807, Mar. 2018, doi: 10.1109/JSTARS.2017.2778076.

[59] J. Tian, X. Zhu, L. Wan, and M. Collin, "Impacts of satellite revisit frequency on spring phenology monitoring of deciduous broad-leaved forests based on vegetation index time series," *IEEE J. Sel. Topics Appl. Earth Observ. Remote Sens.*, vol. 14, pp. 10500–10508, Oct. 2021, doi: 10.1109/JSTARS.2021.3120013.

[60] X. Zhang, M. A. Friedl, and C. B. Schaaf, "Global vegetation phenology from moderate resolution imaging spectroradiometer (MODIS): Evaluation of global patterns and comparison with in situ measurements," *J. Geophysical Res., Biogeosci.*, vol. 111, no. G4, 2006, Art. no. G04017, doi: 10.1029/2006JG000217.

[61] J. Chen, P. Jönsson, M. Tamura, Z. Gu, B. Matsushita, and L. Eklundh, "A simple method for reconstructing a high-quality NDVI time-series data set based on the Savitzky–Golay filter," *Remote Sens. Environ.*, vol. 91, no. 3, pp. 332–344, 2004, doi: 10.1016/j.rse.2004.03.014.
[62] R. Cao et al., "A simple method to improve the quality of NDVI time-series data by integrating spatiotemporal information with the Savitzky-Golay filter," *Remote Sens. Environ.*, vol. 217, pp. 244–257, 2018b, doi: 10.1016/j.rse.2018.08.022.
[63] L. Zeng, B. D. Wardlow, D. Xiang, S. Hu, and D. Li, "A review of vegetation phenological metrics extraction using time-series, multispectral satellite data," *Remote Sens. Environ.*, vol. 237, 2020, Art. no. 111511, doi: 10.1016/j.rse.2019.111511.
[64] X. Zhang et al., "Monitoring vegetation phenology using MODIS," *Remote Sens. Environ.*, vol. 84, no. 3, pp. 471–475, 2003, doi: 10.1016/S0034-4257(02)00135-9.
[65] F. Meng, L. Huang, A. Chen, Y. Zhang, and S. Piao, "Spring and autumn phenology across the Tibetan plateau inferred from normalized difference vegetation index and solar-induced chlorophyll fluorescence," *Big Earth Data*, vol. 5, no. 2, pp. 182–200, 2021, doi: 10.1080/20964471.2021.1920661.
[66] R. Jozefowicz, W. Zaremba, and I. Sutskever, "An empirical exploration of recurrent network architectures," in *Proc. 32nd Int. Conf. Mach. Learn.*, 2015, vol. 37, pp. 2342–2350, Accessed on: Mar. 7, 2023. [Online]. Available: https://www.webofscience.com/wos/woscc/full-record/WOS:000684115800248
[67] L. Li and K. Jamieson, "Hyperband: A novel bandit-based approach to hyperparameter optimization," *J. Mach. Learn. Res.*, vol. 18, pp. 6765–6816, 2017.
[68] KerasTuner, "Kerastuner," 2022. [Online] Available: https://keras.io/kerastuner/
[69] D. P. Kingma and J. L. Ba, "Adam: A method for stochastic optimization," 2014, doi: https://doi.org/10.48550/arXiv.1412.6980.
[70] H. Yuan, X. Wang, R. S. Jassal, L. Lu, J. Peng, and C. Wu, "Remote sensing of autumn phenology by including surface soil temperature: Algorithm development, calibration, and validation," *IEEE J. Sel. Topics Appl. Earth Observ. Remote Sens.*, vol. 15, pp. 6485–6494, Aug. 2022, doi: 10.1109/JSTARS.2022.3196494.
[71] Y. Fu, X. Li, X. Zhou, X. Geng, Y. Guo, and Y. Zhang, "Progress in plant phenology modeling under global climate change," *Sci. China. Earth Sci.*, vol. 63, no. 9, pp. 1237–1247, 2020, doi: 10.1007/s11430-019-9622-2.
[72] E. Fernandez, K. Schiffers, C. Urbach, and E. Luedeling, "Unusually warm winter seasons may compromise the performance of current phenology models—Predicting bloom dates in young apple trees with PhenoFlex," *Agricultural Forest Meteorol.*, vol. 322, 2022, Art. no. 109020, doi: 10.1016/j.agrformet.2022.109020.
[73] T.-F. Yin, L.-L. Zheng, G.-M. Cao, M.-H. Song, and F.-H. Yu, "Species-specific phenological responses to long-term nitrogen fertilization in an alpine meadow," *J. Plant Ecol.*, vol. 10, no. 2, pp. 301–309, 2017, doi: 10.1093/jpe/rtw026.
[74] J. Zhu, Y. Zhang, and Y. Liu, "Effects of short-term grazing exclusion on plant phenology and reproductive succession in a Tibetan alpine meadow," *Sci. Rep.*, vol. 6, 2016, Art. no. 27781, doi: 10.1038/srep27781.
[75] X. Zhang, L. Liu, and D. Yan, "Comparisons of global land surface seasonality and phenology derived from AVHRR, MODIS, and VIIRS data," *J. Geophysical Res., Biogeosci.*, vol. 122, no. 6, pp. 1506–1525, 2017, doi: 10.1002/2017JG003811.

Ruyin Cao received the B.S. degree in resource science and engineering and the Ph.D. degree in geography from Beijing Normal University, Beijing, China, in 2007 and 2013, respectively.

He was a Postdoctor with the National Institute of Environmental Studies, Tsukuba, Japan, from 2013 to 2015. He is currently a Professor with the School of Resources and Environment, University of Electronic Science and Technology of China, Chengdu, China. His current research interests include remote sensing image processing and vegetation parameter retrieval.

Xiaofang Ling received the B.E. degree in space science and technology from the Chengdu University of Technology, Chengdu, China, in 2019, and the M.S. degree in mapping science and technology from the University of Electronic Science and Technology of China, Chengdu, in 2022.

Her research interests include remote sensing image processing and temporal data reconstruction.

Licong Liu received the B.S. degree in spatial information and digital technology from the University of Electronic Science and Technology of China, Chengdu, China, in 2017, and the M.S. degree in nature resources in 2020 from Beijing Normal University, Beijing, China, where he is currently working toward the Ph.D. degree in geographic information science.

His current research interests include remote sensing image processing and monitoring of vegetation dynamic with remote sensing.

Weiyi Wang received the B.E. degree in spatial formation and digital technology in 2022 from the University of Electronic Science and Technology of China, Chengdu, China, where she is currently working toward the Graduate degree in mapping science and technology with the School of Resources and Environment.

Her current research interests include remote sensing of vegetation.

Luchun Li received the B.E. degree in space science and technology, along with the B.A. degree in English, from the Chengdu University of Technology, Chengdu, China, in 2021. She is currently working toward the Graduate degree in mapping science and technology with the School of Resources and Environment, University of Electronic Science and Technology of China, Chengdu.

Her current research interests include remote sensing of crop phenology.

Miaogen Shen received the B.S. degree in physics and the Ph.D. degree in physical geography from Beijing Normal University, Beijing, China, in 2004 and 2009, respectively.

He is a Professor of physical geography with the Faculty of Geographical Science, Beijing Normal University, Beijing, China. His research focuses on responses and feedback of vegetation to climate change, as well as remote sensing of vegetation structural and functional parameters.